Korean J. Chem. Eng., 39(11), 3109-3120 (2022)
DOI: 10.1007/s11814-022-1220-2

pISSN: 0256-1115
eISSN: 1975-7220

Adsorption properties of β-carotene on mesoporous carbon-coated honeycomb monolith: Kinetics, thermodynamics, and regeneration studies

Cai-Kian How*, Soroush Soltani*, Teong-Guan Chuah*,, Eng-Tong Phuah***, and Thomas Shean-Yaw Choong*,**,†**

*Center of Sustainable Research, Department Chemical and Environmental Engineering, Universiti Putra Malaysia, 43400 UPM Serdang, Selangor, Malaysia
**INTROP, Universiti Putra Malaysia, 43400 UPM Serdang, Selangor, Malaysia
***Department of Food Science and Technology, School of Applied Sciences and Mathematics, Universiti Teknologi Brunei, BE1410, Bandar Seri Begawan, Brunei Darussalam
(*Received 24 February 2022 • Revised 17 May 2022 • Accepted 30 June 2022*)

Abstract−A facile synthesis procedure of mesoporous carbons coated monolith (MCCM) adsorbent was accomplished using furfuryl alcohol as carbon precursor, triblock copolymer Pluronic F-127 as the structure-directing agent, pyrrole as the binder for polymerization with nitric acid as catalyst and inorganic cordierite as substrate through dip-coating method. Surface chemistry revealed the dominance of acidic sites over adsorbents surface with the majority of active sites occupied by the phenolic and carboxylic groups. The MCCM adsorbent exhibited representative Type IV isotherm with a uniform-distributed PSD plot centered at 6.18 nm. A thermodynamics study involving Langmuir and Freundlich models was applied to establish the adsorption equilibrium data at temperatures of 30 to 50 °C. The Freundlich model best described the experiment data with maximum adsorption capacity of β-carotene onto MCCM was 192.64 mg/g. Three kinetic models, Lagergren first-order, pseudo-second-order and intra-particle diffusion models, were employed to investigate the adsorption mechanism of β-carotene molecules onto active surface sites of MCCM adsorbent. Both the Lagergren first-order and pseudo-second-order kinetic models fitted with experimental data with the latter described perfectly with higher regression coefficient value (R^2>0.99). Intra-particle diffusion featured the involvement in β-carotene adsorption mechanism, but it was not the sole rate-limiting step. The negative value of Gibbs free energy change (ΔG^o) suggested the spontaneity of β-carotene adsorption process. In contrast, the positive values of enthalpy change (ΔH^o) and entropy change (ΔS^o) demonstrated the endothermic nature and entropy-driven of the adsorption process, respectively. The increased ΔG^o with T indicated an increased degree of spontaneity at high temperatures. Regeneration studies of MCCM adsorbent exemplified a slight decrease in adsorption capacities after three consecutive regeneration cycles.

Keywords: Adsorption Kinetics, Thermodynamics, Regeneration, β-Carotene, Mesoporous Carbons Coated Monolith

INTRODUCTION

Crude palm oil (CPO) is the world's richest natural source of fat-soluble carotenoid pigment which accounts for 500-700 ppm mainly in the form of β-carotene. β-Carotene contributes to intense red-orange color pigment and it is one of the most important naturally occurring antioxidants. Recent studies have shown that carotenoids exhibit anticancer activity against certain cancers such as oral, pharyngeal, lung, and stomach cancers [1]. However, one of the CPO refining objectives is to remove the carotenoid content to produce light-colored edible oils to meet the market demand [2]. During the chemical refining process, adsorptive bleaching clay removes all the undesirable colored compounds, whereas large amounts of carotenoids have been removed by bleaching clay through the physical refining process with the remainder discarded during the deodorization step [3]. Therefore, various methods have been developed to prevent the loss of this natural product, including saponification [4], adsorption using polymeric adsorbents [5,6], selective solvent extraction [7], transesterification followed by both phase separation and molecular distillation of the esters [8,9], nanofiltration membrane technology [10], and supercritical carbon dioxide [11]. Noteworthy that no edible oil is obtained during carotenes recovery *via* the commercially viable transesterification process due to the chemical transformation of triglycerides (TG) to methyl esters [4,6]. To obtain edible oil while separating and concentrating carotenes from crude palm oil, adsorption method was developed by utilizing synthetic polymer adsorbents [5,7-10]. Through the adsorption process, palm carotenes were successfully extracted without undergoing chemical conversion of TG while maintaining the quality of the edible oil.

Activated clay, also termed Fuller's earth, is the most popular adsorbent for purification, decolorization, and stabilization of edible oil as compared to activated carbon and silica-based products due to its cheap price [11-13]. Acid-activated bentonite (AAB) and acid-activated montmorillonite are most commonly being used. However, the adsorption capacity of β-carotene on Fuller's earth

†To whom correspondence should be addressed.
E-mail: csthomas@upm.edu.my

and clay was not as effective as the activated carbon adsorbent. Furthermore, the carotenes were suffering from oxidative or acid-catalyzed degradation reactions.

Several studies for adsorption of β-carotene by using activated carbon adsorbent have been reported [10,14]. In the present study, mesoporous carbons coated onto honeycomb monolith, namely MCCM adsorbent, were prepared by dip-coating method. Adsorbent and catalyst coating on inorganic monoliths have attracted considerable attraction due to their favorable properties, such as low-pressure drop, large geometric surface area, short diffusion lengths, and ease of separation from media without the assistance of an outer magnetic field [15-17]. The adsorption kinetics and mechanisms of β-carotene uptake were modeled at various initial concentrations, whereas isotherms and thermodynamics parameters were calculated to study the adsorption behavior of β-carotene on MCCM at various temperatures. Reusability of MCCM adsorbent after successive regeneration steps was investigated.

MATERIALS AND METHODS

1. Materials

Cordierite monoliths with a channel width of 1.02±0.02 mm and wall thickness of 0.25±0.02 mm were purchased from Beihai Haihuang Chemical Packing Co. Ltd., China. Triblock copolymer poly (ethylene oxide)-*b*-poly(propylene oxide)-*b*-poly(ethylene oxide) Pluronic F-127 ($EO_{106}PO_{70}EO_{106}$) with molecular weights of 13,400 g/mol and synthetic β-carotene (Fig. 1) were purchased from Sigma-Aldrich Inc. Furfuryl alcohol (FA, 98%) and pyrrole (Py, 99%) were obtained from Acros Chemical Inc. Other reagents, such as ethanol (C_2H_5OH, 95%), isopropyl alcohol (IPA, 99%), nitric acid (HNO_3, 65%), dichloromethane (CH_2Cl_2), and acetone (C_3H_6O), were obtained from Systerm Chemical, Malaysia. All chemicals and reagents were as analytical grade or as specified with a high percentage of purity.

2. Methods

2-1. Preparation of MCCM Adsorbents

MCCM adsorbent was used to study the adsorption property of β-carotene. The synthesis method was initiated by mixing 2.5 g of Pluronic F-127 and 5 ml of ethanol followed by the addition of 3 g of FA and 1 g of Py into a reactor equipped with ice bath. After that, 0.2 ml of HNO_3 was added dropwise every 5 min interval into the resulting polymeric resin with continuous magnetic stirring. This step was conducted in an ice bath due to the exothermic nature of the polymerization reaction [18]. By employing the dip-coating method, cordierite monoliths were impregnated into polymerized resin solution and soaked for 24 h [19]. To ensure the homogeneous coating of carbon precursors, pressurized air was applied along the cordierite channels to flush away the plethora of polymeric resin solution trapped. The resultant polymer-supported cordierite was then placed inside a hood for 6 h at ambient temperature to evaporate the excessive ethanol solvent, and the polymer layer was allowed to solidify. Then, carbon precursor coated monolith was thermo-polymerized in an oven at 100 °C for 24 h to ensure complete solidification reaction. It was then carbonized inside a tube furnace at 700 °C for 4 h under purified nitrogen gas flow with a heating rate of 3 °C/min for template decomposition. During the carbonization process, FA precursors were carbonized into a matrix of porous carbon while surfactant was decomposed, and in turn, volatilized leaving behind voids in the form of mesopores. Consequently, an integral carbonaceous framework was formed.

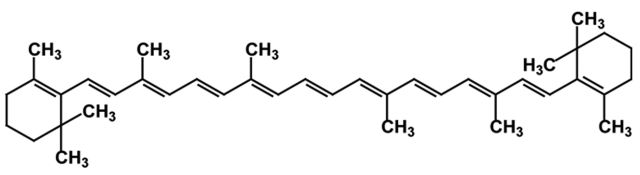

Fig. 1. Structural formula of β-carotene.

2-2. Characterizations of MCCM Adsorbent

The surface morphology of MCCM was captured by using a field emission scanning electron microscope (FE-SEM; JEOL JSM-7600F, Japan) operated at 5.0 kV with magnification ranging from 1,500 to 40,000 x. The X-ray diffraction (XRD) measurements were taken by XRD Shimadzu 6000 diffractometer with CuK_α radiation operating at 40 kV/30 mA and λ–0.1540598 nm. Fourier transform infrared (FT-IR) spectroscopic analysis was performed by using an auxiliary experiment module (AEM) with Nicolet FT-IR Spectrometer. The pore architecture of MCCM for example specific surface area (S_{BET}), pore radius (D_v), total pore volume (V_t), and pore size distribution (PSD) were determined by nitrogen adsorption-desorption isotherm operating at −196 °C using gas sorption analyzer (Sorptomatic Series V1.03). Before each measurement, the MCCM samples were crashed into pieces form and then degassed under vacuum at 290 °C for 9 h.

The acidic and basic surface active sites present on MCCM samples were determined by Boehm's acid-base titration experiments [20]. The total acidic sites were neutralized using alkaline solutions (0.1 N NaOH, 0.1 N $NaHCO_3$, 0.1 N Na_2CO_3), while basic sites were neutralized with 0.1 N HCl solution. The acidic and basic sites were determined by adding 50 ml of 0.1 N titrating solution and 0.5 g of MCCM sample to each 250 ml conical flask. The flasks were agitated inside a water-bath shaker (Stuart SBS40) at 200 rpm under ambient temperature conditions for five days. After that, 10 ml of each sample was titrated with 0.1 N HCl or 0.1 N NaOH solution. The titration was carried out in triplicate using a potentiometer [18,21].

2-3. Preparation and Determination of Adsorbate Stock Solution

One gram of synthetic β-carotene powder was diluted in 1,000 ml of IPA solvent to prepare 1,000 mg/l of standard stock solution. The desired concentrations of experimental samples were then obtained by successive dilutions and their concentrations were measured by using a UV-Vis spectrophotometer. The absorbance of β-carotene before and after adsorption can be calculated through a standard calibration curve of various β-carotene concentrations solution at the wavelength corresponding to the maxima absorbance, λ_{max} of 446 nm. The model calibration equation was y=0.1899x+0.0143 (r^2=0.999).

2-4. Adsorption Studies

The feasibility of MCCM adsorbent for β-carotene sorption process was tested with both batch adsorption and desorption studies. β-Carotene solutions (C_o - 50 to 500 mg/l) were prepared in 250 ml Erlenmeyer flasks by diluting the desired volume of 1,000 mg/l

of stock solution with IPA solvent. β-Carotene solution (V - 200 ml) with 7.0 g of MCCM adsorbent was equilibrated inside a water bath shaker at 150 rpm at 30 °C under nitrogen atmosphere. The Erlenmeyer flask was wrapped with aluminum foil to prevent photodegradation of β-carotene. The sample was left equilibrated for 60 h and residual β-carotene concentration was measured by using UV-Vis spectrophotometer at a maximum wavelength of 446 nm. A control experiment was carried out to check the degradation of β-carotene in the absence of MCCM adsorbent. It was found that there was no remarkable light-degradation of β-carotene inside the Erlenmeyer flask [9].

The equilibrium adsorption capacity (q_e, mg/g) was calculated as below:

$$q_e = (C_o - C_e) \times \frac{V}{m} \quad (1)$$

where C_o and C_e are the initial β-carotene concentration (mg/l) and β-carotene concentration at equilibrium phase (mg/l), respectively, m is the mass of adsorbent (g), and V is the volume of adsorbate solution (l).

Contact time studies were conducted at different β-carotene concentrations at predetermined time intervals and adsorption capacity (q_t, mg/g) at time, t were analyzed. Thermodynamic studies were carried out at different reaction temperatures ranging from 30 to 50 °C.

2-5. Desorption and Regeneration Studies

A preliminary study was done to investigate an appropriate solvent for desorption studies. Three organic solvents, dichloromethane, ethanol and acetone, were used as eluent. For regeneration studies, the MCCM adsorbent was first equilibrated with 500 mg/l of β-carotene in IPA solution. After equilibration, the adsorbent was dried inside an oven at 60 °C overnight. The equilibration time for the adsorption process was 60 h, similar to desorption studies. The saturated MCCM was then washed with distilled water to remove the unabsorbed traces of β-carotene. It was then treated with 100 ml of dichloromethane solvent to elute the adsorbed β-carotene. The aforementioned step was carried out by using an ultrasonic operating at 50 Hz (200 W) and temperature of 30 °C for 8 h [22].

The regenerated monolithic mesoporous carbons were rinsed with distilled water and then dried in an oven. Then again treated with a fresh solution of the adsorbate for the second adsorption with all test conditions remaining the same. After adsorption, the honeycomb monolithic mesoporous carbon adsorbent was taken out for further regeneration. The residue β-carotene solution was analyzed and the adsorption capacity (mg/g) of regenerated β-carotene was calculated. The spent MCCM adsorbent was again regenerated for three consecutive cycles. The regeneration efficiency (%RE) of the MCCM adsorbent was calculated as below:

$$\%\ RE = \frac{\text{Adsorption capacity of regenerated MCCM}}{\text{Adsorption capacity of fresh MCCM}} \times 100\% \quad (2)$$

RESULTS AND DISCUSSION

1. Characterizations of MCCM

The nitrogen adsorption isotherm of MCCM composite and its corresponding PSD plot are presented in Fig. 2. MCCM adsorbent according to IUPAC classification resembled Type IV isotherm, which typically is mesopores-rich texture of carbonaceous materials [23]. A steep and intensive H1-type like hysteresis loop was observed at high relative pressure (P/P_o>0.6), implying superior uniformity and good connectivity of mesopores [24]. Also noteworthy is that the adsorption isotherm leveled off at relative pressure of ~0.9, indicating a small textural mesoporosity of MCCM adsorbent [17]. Meanwhile, its corresponding PSD plot depicted a broad peak with maxima centered at 6.18 nm and mesopores ranging from ~3 to ~15 nm, which further confirmed the assertion of uniform-distributed mesoporosity.

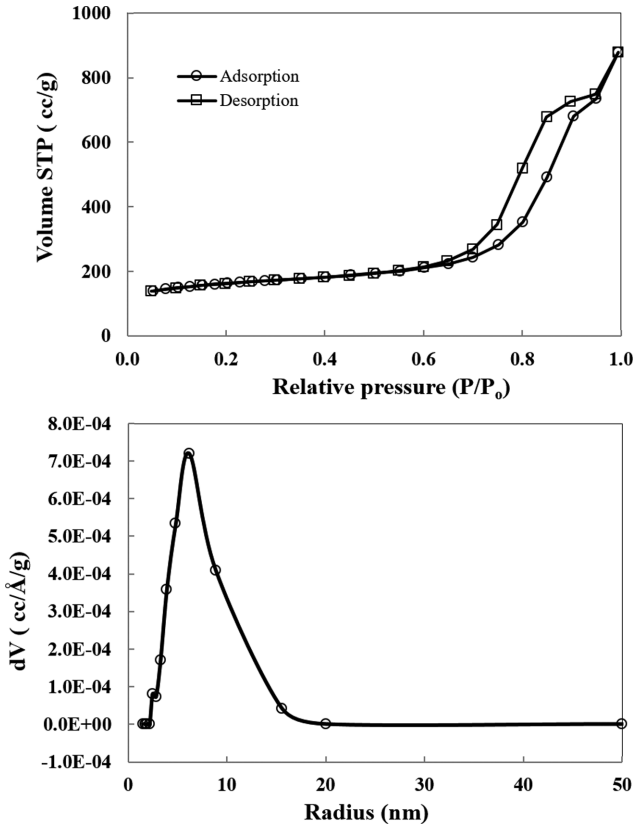

Fig. 2. Nitrogen adsorption isotherm and corresponding PSD curve of MCCM.

Table 1 summarizes the surface chemistry and textural properties of MCCM adsorbent. Boehm's acid-base titration analysis revealed that domination of total acidic sites (1.1138 mmol/g) over the surface of MCCM adsorbent in which phenolic and carboxylic occupied the majority of the composite (Table 1). A higher acidic group leads to more active sites of carbon surface, thus facilitating the uptake of β-carotene molecules [25]. Besides, MCCM exhibited a specific surface area (S_{BET}) coverage of 311.48 m^2/g, while total pore volume (V_t) occupied 0.7976 cm^3/g of the total surface with a pore radius (D_v) of 6.204 nm. Pore sizes and total pore volume are important features that influence the adsorption capacity. Theoretically, larger pore size can accommodate larger molecule species, while greater pore volume can adsorb more chemical species. Garcia-Bordejé suggested that the mesopore range between 5 to 15 nm

Table 1. Surface chemistry and textural properties of MCCM adsorbent

Surface active sites	
Total acidic sites	**1.1138 mmol/g**
Phenolic	0.6454 mmol/g
Carboxylic	0.4109 mmol/g
Lactonic	0.0575 mmol/g
Total basic sites	**0.0137 mmol/g**
Textural properties	
Specific surface area, S_{BET}[a]	311.48 m^2/g
Total pore volume, V_t[b]	0.7976 cm^3/g
Pore radius, $D_v(r)$[c]	6.204 nm
Crystallite size, τ[d]	10.2 nm

[a]BET surface area calculated from experimental points at P/P_o= 0.05-~0.995

[b]Total pore volume obtained from N_2 amount adsorbed at highest P/P_o (~0.995)

[c]Pore radius derived from adsorption branches of isotherms based on BJH model

[d]Crystallite size (τ) calculated from Scherrer Equation by XRD measurement

was found to be the desired compromise between surface area and accessibility for adsorption reactions [15].

The surface functional group of MCCM was investigated by FT-IR interpretation. Fig. 3 exhibits FT-IR spectra for the MCCM adsorbent before the adsorption process. There is a broad band at 3,440 cm^{-1}, assigned to Si-OH group, indicating strong hydrogen bonding (free hydroxyl group) attached to the cordierite framework. The weak peak around 1,628 cm^{-1}, corresponds to aromatic C=O stretching mode from quinine-type carbonyl group in which oxygen atom conjugated with the carbon basal of carbonaceous materials [26]. An intense peak was observed at 1,179 cm^{-1}, attributed to C-O stretching vibration of the phenolic group. The transmittance in the region of 958 to 676 cm^{-1} was ascribed to the vibration of C-H out of plane mode, further confirming the existence of aromatic structures of the carbon basal plane. The spectrum also

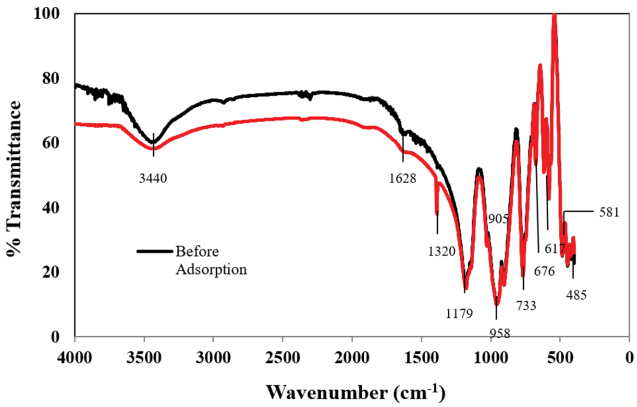

Fig. 3. FT-IR of MCCM adsorbents before and after the adsorption process.

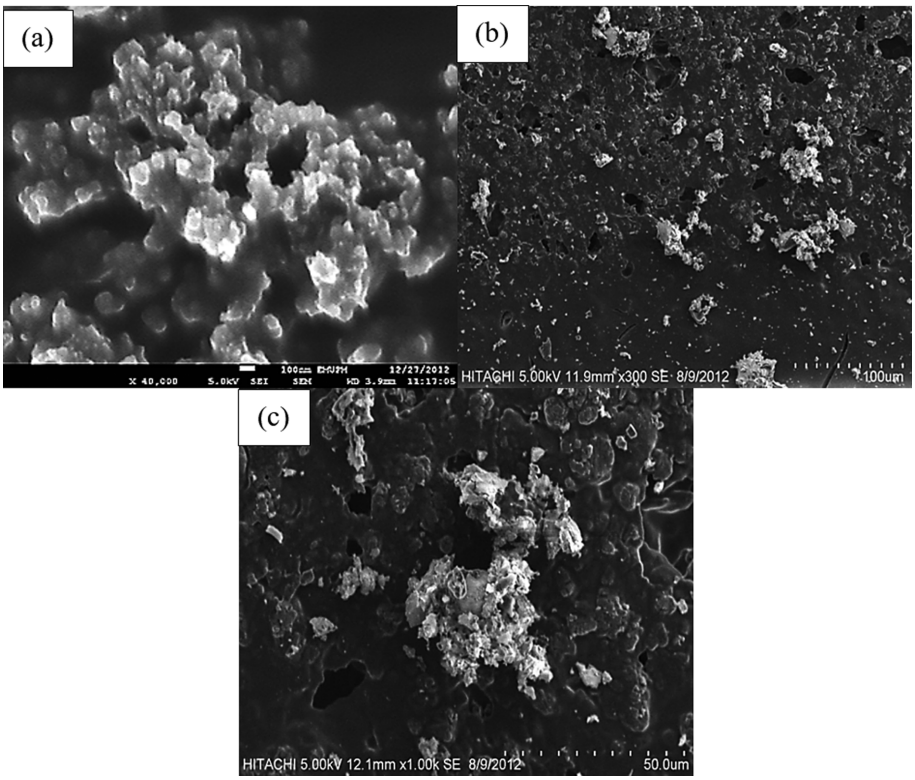

Fig. 4. SEM images of (a) fresh MCCM adsorbent and (b) MCCM adsorbent after adsorption process at 40,000x magnification while (c) blockage of MCCM surface after adsorption.

showed several strong peaks at 617, 581, and 485 cm^{-1} aligned to Si-O stretching bands [27].

However, a drastic decrease in peak intensity at 3,440 cm^{-1} was observed after β-carotene adsorption process, which confirmed the uptake of β-carotene molecules onto the active hydroxyl (-OH) groups over the surface coverage of MCCM. Evidently, the disappearance of the peak at 1,628 cm^{-1} and the formation of a strong peak at 1,320 cm^{-1} were detected after the adsorption process. A strong peak at 1,320 cm^{-1} corresponding to -O-CO-CH_3 stretching mode of acetate esters and the gradual disappearance of peak at 1,628 cm^{-1} could be explained by the slight change of aromatic carboxylic C=O bonding to acetate ester C-O bond in order to facilitate the incorporation of β-carotene molecules.

Fig. 4(a) and (b) illustrate the surface morphology of the MCCM adsorbent before and after adsorption, respectively. The SEM images reveal distributed coverage of carbonaceous materials onto monolithic surface. The fresh MCCM adsorbent displays the skeleton of monolithic carbonaceous material which joined together, building up an interconnected worm-like framework of porous structures [28]. On the other hand, Fig. 4(b) illustrates the widespread distribution of β-carotene crystallites over the surface of MCCM adsorbent after the adsorption process. The blockage of the pores by β-carotene pigmentation is clearly demonstrated in Fig. 4(c).

Fig. 5 illustrates the energy-dispersive X-ray spectroscopy. EDX analysis manifested the existence of magnesium (Mg), aluminum (Al), silicon (Si), and titanium (Ti), which are elemental compositions of cordierite monolith. The weight % of carbon, C, escalated from 12.27% to 27.63% after the adsorption process, attesting to the successful coating of carbonaceous materials. Besides that, observation of reduced weight % of O^{2-} surface active species after adsorption further confirmed the assertion of favorable adsorption features. The finding was consistent with FT-IR spectra of MCCM adsorbent where there was a drop in the peak intensity at 3,440 cm^{-1} after the adsorption process, suggesting the depletion of the adsorption active sites (-OH functional group) on MCCM (Fig. 3). It was further proven by the coverage of the β-carotene crystallites over the surface of MCCM as illustrated in Fig. 4(b).

The inset of Fig. 6 shows several distinct XRD peaks at 2θ ranging from 10 to 70°. There is only very little amorphous scattering inside XRD pattern, thus confirming the crystalline structure of MCCM materials. The most intense peaks appear at 10.5° followed by 18°, 22°, 26.5°, 28.5°, 29.5°, 34° and 54°, reflecting hkl index of (1 0 0), (1 1 0), (1 0 2), (1 1 2), (2 0 2), (2 1 1), (2 1 2) and (2 2 4) plane, respectively. The mean crystallite size of the MCCM sample is 10.2 nm which was calculated by using the Debye-Scherrer equation as shown below:

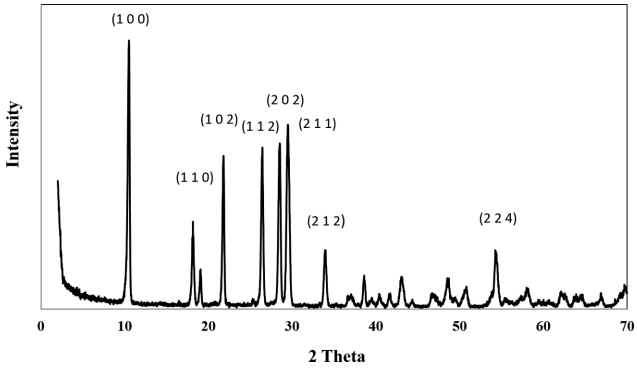

Fig. 6. X-ray diffraction pattern of MCCM adsorbent.

$$\tau = \frac{K\lambda}{\beta \cos\theta_\beta} \quad (3)$$

where K is Scherrer constant (K - 0.89), λ is X-ray wavelength (λ - 0.1540598 nm), θ_β is Bragg diffraction angle, and β is the line broadening at full width half maximum (FWHM in radians), and τ is mean crystalline domains.

2. Effect of Contact Time at Various Initial Concentrations

Contact time was studied to determine the equilibrium time for different initial concentrations at reaction temperature of 30 °C. Fig. 7 shows two regimes of adsorption stages which initiated with a rapid increment in amount of β-carotene adsorbed (q_t) as function of adsorption time and then slowed as it approached the equilibrium stage. This can be explained by the rapid attachment of β-carotene pigmentation onto MCCM surface at the initial stage of

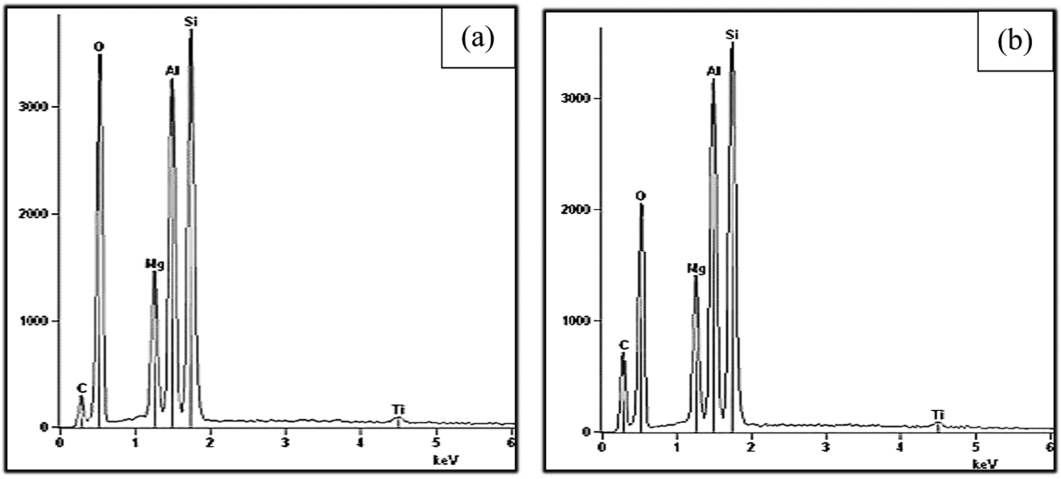

Fig. 5. EDX spectra of (a) before and (b) after β-carotene adsorption process.

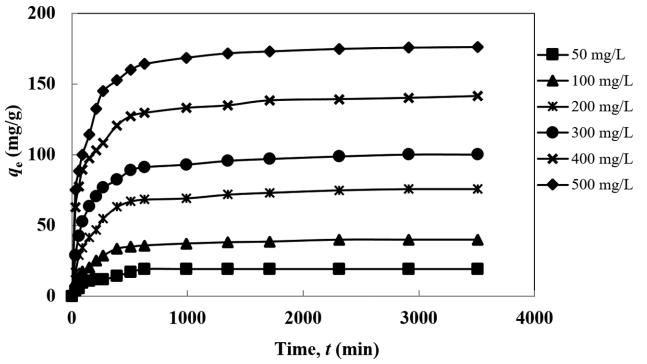

Fig. 7. Adsorption capacities versus time of various initial β-carotene concentrations at T=30 °C.

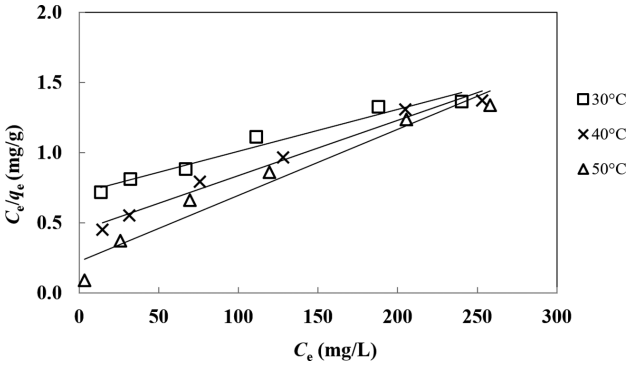

Fig. 8. The linearized Langmuir isotherm plots for β-carotene adsorption on MCCM at various temperatures (agitation speed - 150 rpm).

the adsorption process until the available adsorption sites were gradually occupied [8].

The maximum adsorption capacity of β-carotene onto MCCM at equilibrium time (q_e) increased from 19 to 171 mg/g as initial concentration ranged from 50 to 500 mg/g. The increase in initial concentration stimulated a significant mass driving force to overcome all mass transfer resistances of the adsorbate between the liquid and solid phases [7]. Therefore, more pigment molecules could diffuse from the bulk solution to the MCCM surface.

It was observed that higher initial concentration took a relatively longer contact time to reach the equilibrium stage as a higher amount of adsorbate was required to encounter the first boundary layer effect before diffusing from the boundary layer film onto the adsorbent surface. Finally, it would pass through the porous structure of the adsorbent [29].

3. Adsorption Equilibrium Isotherms

Two common adsorption isotherms, Langmuir and Freundlich models, were used to investigate the relation between the amounts of a solute adsorbed at a constant temperature and its concentration in the equilibrium solution. To optimize the design of an adsorption system, it is essential to establish the most appropriate correlation for the equilibrium data.

Langmuir isotherm model is most widely used to describe the sorption process and a few assumptions have been adopted [30]. The model describes monolayer chemisorption onto distinct sites of an idealized adsorbent at the equilibrium stage. The adsorbent has a finite number of active sites for adsorbate uptake. Thus, only one adsorbate molecule occupies an active site without interaction between molecules of the adjacent sites. No further adsorption can occur once all the active sites have been fully occupied (saturation point reached). Langmuir isotherm model also assumes that the sorption process occurs at a specific homogeneous adsorbent with all sites identical and energetically equivalent.

The equation of Langmuir isotherm can be represented as follows.

$$q_e = \frac{x}{m} = \frac{bK_L C_e}{1+K_L C_e} = \frac{KC_e}{1+a_L C_e} \tag{4}$$

The linearized form can be expressed as:

$$\frac{C_e}{q_e} = \frac{1}{K_L b} + \frac{C_e}{b} = \frac{1}{K} + \frac{a_L C_e}{K} \tag{5}$$

where x (mg) is the amount of β-carotene adsorbed, m (g) is mass of mesoporous carbon coated used, K (L/g) is the Langmuir isotherm constant, K_L (L/mg) is the Langmuir isotherm constant related to the affinity of the binding sites or net enthalpy of adsorption and equal to a_L and b (mg/g) is the theoretical monolayer capacity (maximum adsorption capacity) of the adsorbent and equal to K/a_L while C_e (mg/l) and q_e (mg/g) are concentration and adsorption capacity of β-carotene at equilibrium, respectively. The value of K_L and b can be obtained from the intercept and slope of the linear plot of C_e/q_e versus C_e, respectively (Fig. 8).

The main features of the Langmuir isotherm can be expressed in terms of a dimensionless constant known as separation factor, also called equilibrium parameter (R_L) which is defined as below [31].

$$R_L = \frac{1}{1+K_L C_o} \tag{6}$$

where C_o is the initial concentration of β-carotene (mg/l) and K_L is the Langmuir constant related to the energy of adsorption (L/mg). The value of R_L indicates the shape of the isotherms to be either favorable ($0<R_L<1$), unfavorable ($R_L>1$), linear ($R_L=1$) or irreversible ($R_L=0$).

The Freundlich isotherm is the earliest developed isotherm model that evaluates the sorption equation [32]. The model describes the adsorption equilibrium on heterogeneous surfaces with interaction between adsorbed molecules. In addition, the application of the Freundlich equation also suggests the inequality of adsorption energy over the surface of all adsorption sites.

The Freundlich isotherm can be expressed as:

$$q_e = k_F C_e^{1/n} \tag{7}$$

While the linearized form can be expressed as:

$$\log q_e = \log k_F + \frac{1}{n}\log C_e \tag{8}$$

where k_F (L/mg) is the Freundlich isotherm constant related to the bonding energy and can be defined as the adsorption or distribution coefficient, which describes the quantity of β-carotene adsorbed onto MCCM surface for a unit equilibrium concentration while 1/n is the heterogeneity factor. The graph of $\log q_e$ against $\log C_e$ is

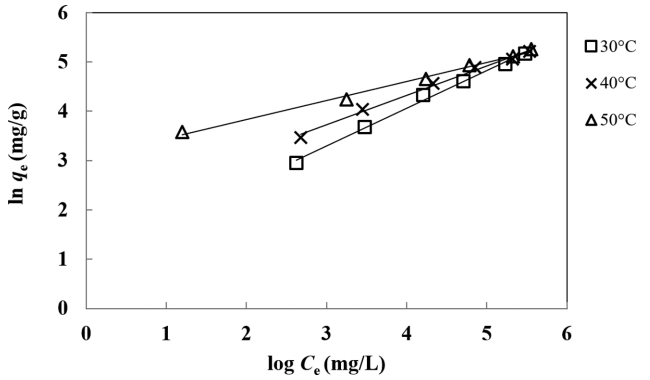

Fig. 9. The linearized Freundlich isotherm plots for β-carotene adsorption on MCCM at various temperatures (agitation speed - 150 rpm).

Table 2. Langmuir and Freundlich isotherm constants for β-carotene adsorption on MCCM at various temperatures

Isotherm	Parameters	30 °C	40 °C	50 °C
Langmuir	q_m (mg/g)	176.05	184.52	192.64
	K_L (l/mg)	0.0042	0.0088	0.0206
	R_L	0.32	0.19	0.09
	R^2	0.9626	0.9812	0.9553
	X^2	0.009	0.012	0.125
Freundlich	k_F (mg/g)(l/mg)$^{1/n}$	2.76	6.86	21.37
	1/n	0.7619	0.5989	0.3859
	R^2	0.9946	0.9932	0.9925
	X^2	0.003	0.004	0.005

employed to generate the slope of 1/n and intercept of logk_F as shown in Fig. 9. The value of 1/n in the range of 0 to 1 indicates the favorability of the adsorption process. However, a value for 1/n below than one shows a normal Langmuir isotherm while 1/n above one indicates cooperative adsorption [33].

As presented in Table 2, the values of R_L were between 0.09 to 0.32, implying favorable nature of the adsorption process. Meanwhile, the values of 1/n fell in the range of 0.39 to 0.76, which further confirms the favorability of the adsorption process. The Freundlich constant, k_F increased to a greater extent with the rise in temperature. In general, a larger k_F value indicates a higher affinity for β-carotene molecules, consequently a more effective adsorption process [34]. An increase in temperature increases the diffusion rate of β-carotene molecules onto the adsorbent surfaces, allowing the uptake of molecules into pores more readily. The applicability of both isotherms was determined by comparing the values of the correlation coefficients, R^2, of corresponding linearized plots. From Table 2, the experimental adsorption data fitted both Langmuir and Freundlich isotherm models. However, the latter described the best with values of R^2>0.99. Similarly, Boki et al. [35] proposed that the Freundlich isotherm was more applicable to describe the adsorption of β-carotene pigment extracted from various vegetable oils using bentonite, montmorillonite, and sepiolite adsorbent [35]. Also, Boki et al. [36] suggested that the Freundlich isotherm yields a better fit than the Langmuir in describing the adsorption of carotenoid pigments from rapeseed and soybean oil onto standard bleaching clays, synthetic adsorbents, and attapulgites adsorbent [36]. Besides that, the adsorption of β-carotene from crude maize and sunflower oil using acid-activated bentonite (AAB) followed the Freundlich isotherm model as well [37].

4. Adsorption Kinetics and Mechanisms

Two common kinetic models, Lagergren first-order [38] and pseudo-second-order [39], were used to evaluate the adsorption kinetics data where uptake rate and equilibrium time of the adsorption process can be identified quantitatively. Meanwhile, the adsorption mechanism of β-carotene molecules onto the surface active sites of MCCM adsorbent was investigated using the intra-particle diffusion model [40].

Lagergren first-order kinetic (1898) is generally expressed as:

$$\frac{dq_t}{dt} = k_1(q_e - q_t) \tag{9}$$

where q_e is the adsorbed amount (mg/g) at equilibrium and k_1 is the rate constant of Lagergren first-order sorption (min^{-1}).

However, after integration and applying the boundary condition at t=0 to t=t and q_t=0 to q_t=q_t, the integrated formulation equation becomes:

$$\log(q_e - q_t) = \log q_e - \frac{k_1 t}{2.303} \tag{10}$$

where q_e and q_t are amount of β-carotene adsorbed onto MCCM at equilibrium and at time t, respectively,, while k_1 is rate constant. The values of k_1, q_e and correlation coefficient R^2 can be determined from the plot of log(q_e−q_t) versus t.

The pseudo-second-order kinetics is expressed as follows:

$$\frac{dq_t}{dt} = k_2(q_e - q_t)^2 \tag{11}$$

where k_2 is the rate constant of pseudo-second-order sorption (g mg^{-1} min^{-1}). By integrating Eq. (12) and applying the boundary condition at t=0 to t=t and q_t=0 to q_t=q_t, the integrated formulation equation becomes:

$$\frac{t}{q_t} = \frac{1}{k_2 q_e^2} + \frac{t}{q_e} \tag{12}$$

The values of k_2 and q_e can be determined by plotting the graph of t/q_t versus t, where the slope and intercept of the linearized pseudo-second-order equation are k_2, rate constant for pseudo-second-order and q_e, adsorption capacity, respectively.

The applicability of both kinetic models was investigated by comparing the regression coefficients (R^2) of both linearized plots. The experimental data for β-carotene adsorption of various initial concentrations at 30 °C were fitted by both Lagergren first-order and pseudo-second-order equations with R^2 values higher than 0.9, and the values of k_1, k_2, q_e and R^2 are listed in Table 3. The linearized plot of log (q_e−q_t) versus t and graph of t/q_t versus t are presented in Figs. 10 and 11, respectively.

As shown in Table 3, the pseudo-second-order kinetic model yielded a higher regression coefficient (R^2>0.997) compared with the Lagergren first-order kinetic model. This can be further veri-

Table 3. Kinetics parameters for β-carotene adsorption at various initial concentrations on MCCM adsorbent at T=30 °C

C_o (mg/L)	$q_{e,exp}$ (mg/g)	Largregren first-order			Pseudo-second-order		
		$q_{e,calc}$ (mg/g)	$k_1\times10^{-3}$ (min^{-1})	R^2	$q_{e,calc}$ (mg/g)	$k_2\times10^{-5}$ (g/mg min)	R^2
50	19.20	14.92	4.38	0.9407	20.00	47.07	0.9976
100	39.70	29.84	4.84	0.9763	40.98	23.95	0.9991
200	75.70	56.10	4.84	0.9858	78.13	12.71	0.9992
300	100.09	63.42	4.61	0.9850	102.04	12.44	0.9996
400	141.35	71.58	4.15	0.9793	142.86	11.69	0.9996
500	176.05	94.23	4.61	0.9596	178.57	8.96	0.9997

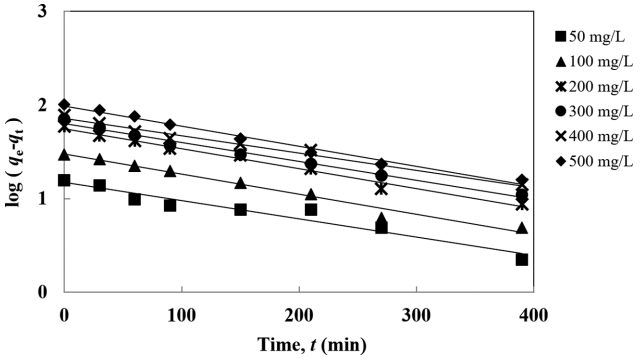

Fig. 10. The Lagergren first-order adsorption kinetic of β-carotene at various initial concentrations in IPA solution at T=30 °C.

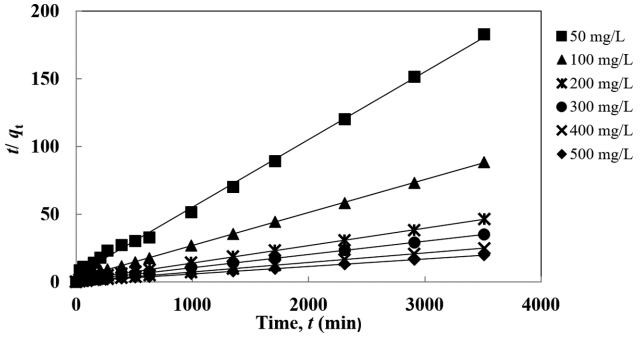

Fig. 11. The pseudo-second-order adsorption kinetic of β-carotene at various initial concentrations in IPA solution at T=30 °C.

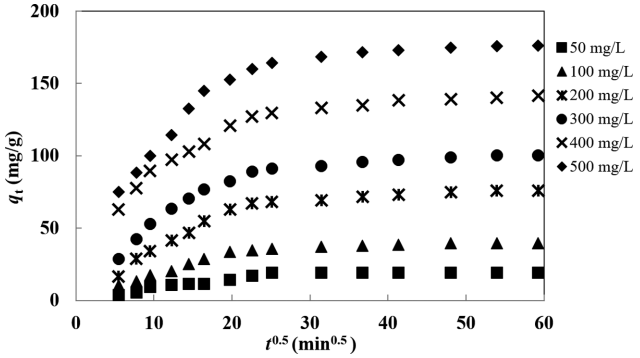

Fig. 12. The Weber and Morris intraparticle diffusion plots for adsorption mechanism of β-carotene at various initial concentrations in IPA solution at T=30 °C.

fied by comparing the theoretical adsorption capacity, $q_{e,calc}$ with experimental adsorption capacity, $q_{e,exp}$ value, computed from both kinetic equations. The obtained result obviously showd that $q_{e,exp}$ of pseudo-second-order model was far more consistent than $q_{e,exp}$ of Lagergren first-order kinetic model. Therefore, it was concluded that the adsorption kinetics of β-carotene onto mesoporous carbons coated monolith was best fitted by the pseudo-second-order kinetic model, suggesting that the adsorption process is a chemisorption process. The adsorption process principally involves a chemical interaction via valence forces by sharing electrons or exchanging the proton between β-carotene molecules and the surface of MCCM until the surface functional sites are fully occupied [7]. Sarier and Güler [41] and Christidis and Kosiari [37] have reported that β-carotene adsorption on the activated clay occurred most likely through a chemical process stemming from the interaction of β-carotene with Lewis and Bronsted acid sites of acid-activated montmorillonite [37,41]. Wu and others [9] reported that adsorption kinetic of β-carotene onto acid-activated bentonite adsorbent in xylene solution followed the pseudo-second-order with correlation coefficient R^2 higher than 0.999 [9]. Ahmad et al. [8] proposed that the pseudo-second-order model describes well the kinetic adsorption of β-carotene onto silica gel and florisil in *n*-hexane solution [8].

Intra-particle diffusion model by Weber and Morris [40] was used to analyze the mass transfer resistance for the uptake of β-carotene molecules onto the active sites of MCCM adsorbent [40]. According to Weber and Morris, the uptake varies almost proportionally with $t^{1/2}$ which is expressed by Eq. (13).

$$q_t = k_i t^{1/2} + C \quad (13)$$

where k_i and C are the intra-particle diffusion rate constant (mg/g $min^{1/2}$) and intercept, respectively. The values of k_i are obtained from the slope of q_t versus $t^{1/2}$ plot as presented in Fig. 12.

The intra-particle diffusion model has three general stages: initial curved portion, followed by linear portion, and lastly plateau portion. The initial curved portion is attributed to the diffusion of adsorbate molecules through the bulk solution to the external surface of the adsorbent (bulk diffusion). The linear portion is the gradual diffusion of the adsorbate molecules from the surface to the internal pores of the adsorbent (particle diffusion or pore diffusion). The plateau portion is the final equilibrium stage where intraparticle diffusion starts to slow due to the extremely low concen-

Table 4. Intra-particle diffusion parameters for β-carotene adsorption at various initial concentrations on MCCM adsorbent at T=30 °C

C_o	k_i (mg/g $min^{1/2}$)	R^2
50	0.6229	0.9278
100	1.1339	0.9088
200	2.1053	0.8903
300	2.4814	0.8751
400	2.7081	0.9088
500	3.6452	0.8723

tration of adsorbate in the solutions as well as the reduced number of available active sorption sites on the MCCM surface [33,42-44].

Intra-particle diffusion model was applied to determine the rate-limiting step of the adsorption process. Hence, for intra-particle diffusion to occur, the plot of q_t versus $t^{1/2}$ should pass through the origin with R^2 value close to unity. Then the rate-limiting process can be considered to be fully controlled by intra-particle diffusion. Otherwise, some other mechanism along with intra-particle diffusion may also be involved. In this study, the Weber and Morris plot (Fig. 12) did not pass through the origin, implying that intra-particle diffusion applied to this system but was not the sole rate-limiting step in the adsorption process. This can be further confirmed by the relatively low regression coefficient of various initial concentrations (R^2<0.9), deviating from the theoretical R^2≈1, thus suggesting two or more steps in the adsorption mechanism. As shown in Table 4, the value of intra-particle diffusion rate, k_i, increases with initial β-carotene concentration. This could be explained by the presence of more β-carotene molecules in the bulk solution which competitively occupy the active sites on MCCM surface.

Generally, the adsorption of β-carotene onto the active sites of mesoporous carbon coated monolith adsorbent is mainly governed by two adsorption stages: liquid phase mass transfer rate and intra-particle mass transfer rate. The first region in the q_t versus $t^{1/2}$ plot is where the adsorption rate is rapid due to the diffusion of β-carotene molecules to the external surface of MCCM adsorbent, subsequently causing an immediate seizing of active surface sites of the adsorbent (liquid phase mass transfer rate). The latter stage in Fig. 12 is the slowest, also known as the rate-limiting step. In this region, the adsorption process is being controlled by intra-particle diffusion, hence slowing the adsorption rate (intra-particle mass transfer rate) [45]. Therefore, in conclusion, the adsorption mechanism of β-carotene was controlled by external mass transfer at the beginning of the process and then intra-particle diffusion at the final stage [46,47].

5. Thermodynamic Studies

The data obtained from the adsorption isotherm model can be used to identify the thermodynamic parameters, such as Gibbs free energy change (ΔG^o), enthalpy change (ΔH^o) and entropy change (ΔS^o). These parameters can be determined by applying the following equation:

$$K_d = k_F = X \tag{14}$$

where K_d (L/mol) is the sorption distribution coefficient. The value of K_d was substituted into Eq. (15) to determine the free energy of the adsorption system at different temperatures.

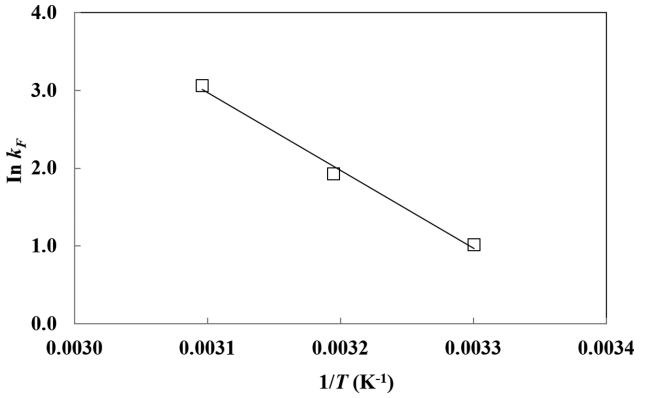

Fig. 13. The van't Hoff plot for adsorption of β-carotene onto MCCM in IPA solvent at different temperatures.

Table 5. Thermodynamic parameters for adsorption of β-carotene onto MCCM at various temperatures

T (K)	ΔG^o (kJ/mol)	ΔH^o (kJ/mol)	ΔS^o (J/mol K)
303	−2.56		
313	−5.01	83.19	282.59
323	−8.22		

The Gibbs free energy changes of the adsorption process at various temperatures were computed using the equation below:

$$\Delta G^o = -RT\ln k_F \tag{15}$$

Whereas the values of enthalpy change and entropy change were shown as follows [48]:

$$\ln k_F = -\frac{\Delta H^o}{RT} + \frac{\Delta S^o}{R} \tag{16}$$

where k_F is adsorption equilibrium constant obtained from the Freundlich isotherm model (Table 2), R is the universal gas constant (8.314 J/mol K), and T is the absolute temperature in Kelvin (K). The values of ΔH^o and ΔS^o were obtained from the slope and intercept of the plot of $\ln k_F$ versus 1/T.

The van't Hoff plot (Fig. 13) was used to evaluate thermodynamic parameters for the sorption system of β-carotene at 30, 40 and 50 °C. From Table 5, the negative values of ΔG^o indicate the favorability and spontaneous nature of β-carotene adsorption on the MCCM adsorbent. Results demonstrated that Gibbs free energy became more negative with the increase in temperature, indicating that the adsorption process is more favorable at a higher temperature. High temperature tends to enhance the affinity between β-carotene molecules and the MCCM surface, thus increasing the degree of spontaneity. The positive value of ΔH^o reveals the endothermic nature of the adsorption process. This result is in agreement with the increased adsorption capacity (q_e) from 176.05 to 192.64 mg/g with the increase in temperature from 30 to 50 °C. Meanwhile, the positive value of ΔS^o implies an increasing disorder and randomness at the solid-solution interface during the adsorption of the β-carotene molecules on the active site of the MCCM

Table 6. Effect of different eluents for desorption studies of various initial β-carotene concentrations solution

Desorbing agent	Concentrations (mg/l)	β-Carotene loading on MCCM (mg/g)		Desorption capacity, ($q_i - q_e$)	Desorption efficiency (% q_{des})
		Adsorption, q_i	Desorption, q_e		
Dichloromethane	50	30.76	22.63	8.14	26.45
	100	74.79	50.90	23.89	31.94
	200	106.85	71.49	35.35	33.09
	300	137.95	89.97	47.98	34.78
	400	163.70	105.25	58.46	35.71
	500	173.59	107.71	65.88	37.95
Acetone	50	36.44	28.79	7.65	20.99
	100	63.09	49.78	13.31	21.09
	200	68.44	53.02	15.42	22.53
	300	86.79	67.23	19.56	22.54
	400	136.42	105.56	30.87	22.63
	500	138.17	105.71	32.46	23.50
Ethanol	50	35.67	29.55	6.11	17.15
	100	65.50	53.06	12.45	19.00
	200	83.28	66.78	16.50	19.81
	300	101.49	81.37	20.12	19.82
	400	127.37	101.88	25.49	20.01
	500	157.05	125.38	31.67	20.16

adsorbent. This is due to energy redistribution between the adsorbate and the adsorbent [43]. Therefore, the adsorption process is endothermic ($\Delta H^o>0$) with positive entropy change ($\Delta S^o>0$), and the process will therefore become spontaneous at high temperatures (>22 °C).

6. Desorption and Regeneration Studies

6-1. Solvent Selection for Desorbing Agent

A preliminary study was carried out to check the ability of three different desorbing agents to elute the β-carotene from MCCM adsorbent in isopropyl alcohol solution after the adsorption process. This study used three chemical reagents, dichloromethane, acetone and ethanol, as an eluent. The desorption process was carried out using an ultrasonic (50 Hz, 200 W) at a temperature of 30 °C for 8 h when the equilibrium was reached. The results are shown in Table 6. From Fig. 14, the maximum desorption capacity of β-carotene when dichloromethane was used as an eluent at a concentration of 500 mg/l which was 65.88 mg/g. The desorption efficiency of β-carotene increased with increasing initial β-carotene concentration, as depicted in Fig. 15. Dichloromethane solvent showed the highest % desorption efficiency followed by acetone, while ethanol had the least value. β-Carotene is a nearly non-polar compound and its extraction could be enhanced by using polar aprotic (semi-polar) solvents, such as dichloromethane and acetone solvent. These solvents were found to have advantages over several polar or non-polar solvents, for example, methanol, ethanol and diethyl ether. This result is in agreement with Biswas et al. [49] that acetone (moderately polar) solvent is suitable for exaction of β-carotene from carrot and sweet potato samples [49].

6-2. Regeneration Studies

To check the economic feasibility of an adsorption process, the reusability of the adsorbent was investigated through chemical regeneration approaches. For chemical regeneration studies, since dichloromethane solvent gave the highest desorption efficiency, it was

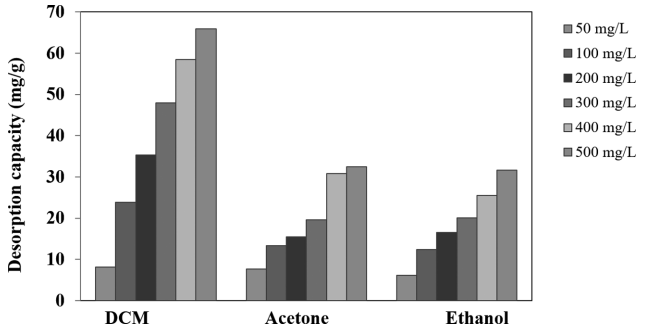

Fig. 14. The desorption capacity of various initial β-carotene concentrations onto MCCM adsorbent by using different eluents.

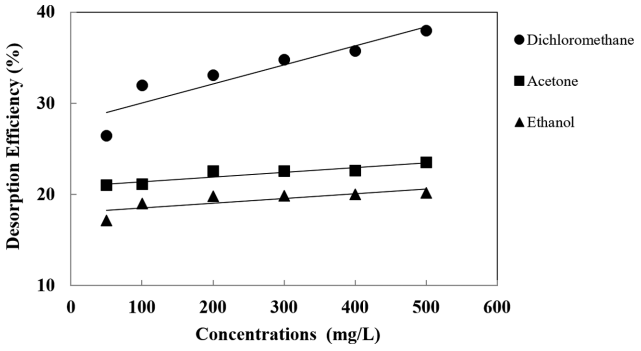

Fig. 15. Desorption efficiency plot of various initial β-carotene concentrations by using different kinds of eluents.

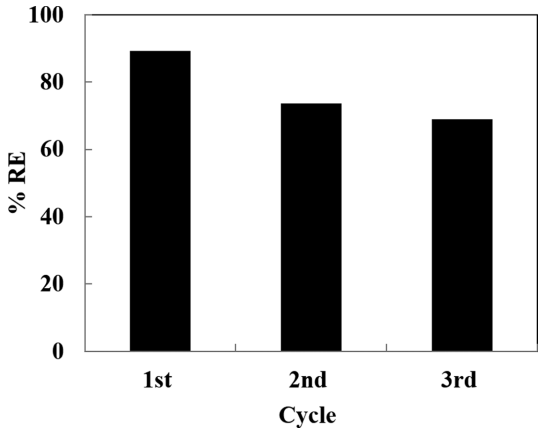

Fig. 16. Regeneration efficiency plot of MCCM adsorbent by using dichloromethane as eluents.

utilized as the eluent for the adsorption process of 500 mg/l of β-carotene solution at 30 °C using an ultrasonic.

Fig. 16 demonstrates a decrease in regeneration efficiency (% RE) of MCCM adsorbent after three consecutive regeneration cycles. In the first cycle, the value of % RE is 89.28% and further decreases to 73.70% and 68.98% for the second and third cycles, respectively. The decrease in adsorption capacity of regenerated β-carotene on MCCM after first regeneration exemplifies a drop in % RE for successive regeneration steps. This might be due to the decomposition of surface adsorption sites or functional groups caused by dichloromethane solvent [50]. Noteworthy that there is only a slight drop in % RE after the second regeneration cycle, which is 4.72%. Therefore, it was believed that MCCM adsorbent could be reused for the adsorption process of β-carotene with slight decreases in adsorption capacities.

CONCLUSION

Mesoporous carbons coated onto hierarchical honeycomb monolith were prepared using triblock copolymer Pluronic F-127 as the structure-directing agent through evaporative induced self-assembly approach. The adsorption behavior of β-carotene and the reusability of MCCM adsorbent were studied. Characterization studies showed the dominance of mesoporosity on the surface of MCCM adsorbent with the most probable size of approximately 6 nm. The equilibrium data were modelled using Freundlich isotherm approach and the thermodynamic parameters further demonstrated β-carotene adsorption onto MCCM was spontaneous, endothermic and entropy-driven. Pseudo-second-order model was found to be best fitted with the adsorption kinetic data, thus exemplifying the incorporation of β-carotene onto pores through chemisorption. Regeneration studies indicated the reusability of MCCM adsorbent after three consecutive cycles for the sorption process of β-carotene without any further activation, and a slight drop in adsorption capacity was observed after successive regenerations.

ACKNOWLEDGEMENTS

The authors would like to thank Universiti Putra Malaysia for financial support via Geran Putra Berimpak (UPM.RMC.800-3/3/1/GPB/2021/9696400).

REFERENCES

1. K. Sundram, R. Sambanthamurthi and Y. A. Tan, *Asia Pac. J. Clin. Nutr.*, **12**, 355 (2003).
2. O. M. Lai, E. T. Phuah, Y. Y. Lee and Y. Basiron, *Palm Oil. Bailey's industrial oil and fat products*, John Wiley & Sons, New Jersey (2020).
3. K. Y. Liew, A. H. Yee and M. R. Nordin, *J. Am. Oil Chem. Soc.*, **70**, 539 (1993).
4. C. K. Ooi, Y. M. Choo, S. C. Yap, Y. Basiron and A. S. H. Ong, *J. Am. Oil Chem. Soc.*, **71**, 423 (1994).
5. B. S. Baharin, K. Abdul Rahman, M. I. Abdul Karim, T. Oyaizu, K. Tanaka, Y. Tanaka and S. Takagi, *J. Am. Oil Chem. Soc.*, **75**, 399 (1998).
6. R. A. Latip, B. S. Baharin, Y. B. Che Man and R. A. Rahman, *J. Am. Oil Chem. Soc.*, **78**, 83 (2001).
7. J. Tong, Z. Wu, X. Sun, X. Xu and C. Li, *Chin. J. Chem. Eng.*, **16**, 270 (2008).
8. A. L. Ahmad, C. Y. Chan, S. R. Abd Shukor and M. D. Mashitah, *Chem. Eng. J.*, **148**, 378 (2009).
9. Z. Wu and C. Li, *J. Hazard. Mater.*, **171**, 582 (2009).
10. M. Muhammad, T. S. Y. Choong, T. G. Chuah, R. Yunus and Y. H. T. Yap, *Chem. Eng. J.*, **164**, 178 (2010).
11. S. C. Kheok and E. E. Lim, *J. Am. Oil Chem. Soc.*, **59**, 129 (1982).
12. P. Falaras, I. Kovanis, F. Lezou and G. Seiragakis, *Clay Miner.*, **34**, 221 (1999).
13. K. S. Low, K. S., C. K. Lee and L. Y. Kong, *J. Chem. Technol. Biotechnol.*, **72**, 67 (1998).
14. M. Z. B. Hussein, D. Kuang, Z. Zainal and T. K. Teck, *J. Colloid Interface Sci.*, **235**, 93 (2001).
15. E. García-Bordejé, F. Kapteijn and J. A. Moulijn, *Carbon*, **40**, 1079 (2002).
16. E. García-Bordejé, M. J. Lázaro, R. Moliner, P. M. Álvarez, V. Gómez-Serrano and J. L. G. Fierro, *Carbon*, **44**, 407 (2006).
17. K. P. Gierszal and M. Jaroniec, *J. Am. Oil Chem. Soc.*, **128**, 10026 (2006).
18. W. Cheah, S. K. Hosseini, M. A. Khan, T. G. Chuah and T. S. Y. Choong, *Chem. Eng. J.*, **215**, 747 (2013).
19. K. M. de Lathouder, J. Bakker, M. T. Kreutzer, F. Kapteijn, J. A. Moulijn and S. A. Wallin, *Chem. Eng. Sci.*, **59**, 5027 (2004).
20. S. L. Goertzen, K. D. Thériault, A. M. Oickle, A. C. Tarasuk and H. A. Andreas, *Carbon*, **48**, 1252 (2010).
21. S. Hosseini, M. A. Khan, M. R. Malekbala, W. Cheah and T. S. Y. Choong, *Chem. Eng. J.*, **171**, 1124 (2011).
22. Y. Wan, X. Cui and Z. Wen, *J. Hazard. Mater.*, **198**, 216 (2011).
23. M. Kruk, M. Jaroniec, C. H. Ko and R. Ryong, *Chem. Mater.*, **12**, 1961 (2000).
24. R. Ryoo, S. H. Joo, M. Kruk and M. Jaroniec, *Adv. Mater.*, **13**, 677 (2001).
25. Y. P. Teoh, M. A. Khan and T. S. Y. Choong, *Chem. Eng. J.*, **217**, 248 (2013).
26. Y. F. Jia and K. M. Thomas, *Langmuir*, **16**, 1114 (2000).
27. Y. Chen, Q. Chen, L. Song, H. P. Li and F. Z. Hou, *Micropor. Meso-*

por. Mater., **122**, 7 (2009).
28. G. P. Hao, W. C. Li, S. Wang, G. H. Wang, L. Qi and A. H. Lu, *Carbon*, **49**, 3762 (2011).
29. I. A. W. Tan, A. L. Ahmad and B. H. Hameed, *J. Hazard. Mater.*, **154**, 337 (2008).
30. I. Langmuir, *J. Am. Oil Chem. Soc.*, **38**, 2221 (1916).
31. G. McKay, M. J. Bino and A. R. Altamemi, *Water Res.*, **19**, 491 (1985).
32. H. Freundlich, *J. Phys. Chem.*, **57**, 1100 (1906).
33. K. Fytianos, E. Voudrias and E. Kokkalis, *Chemosphere*, **40**, 3 (2000).
34. G. Kaynak, M. Ersoz and H. Kara, *J. Colloid Interface Sci.*, **280**, 131 (2004).
35. K. Boki, M. Kubo, N. Kawasaki and H. Mori, *J. Am. Oil Chem. Soc.*, **69**, 372 (1992).
36. K. Boki, H. Mori and N. Kawasaki, *J. Am. Oil Chem. Soc.*, **71**, 595 (1994).
37. G. E. Christidis and S. Kosiari, *Clays Clay Miner.*, **51**, 327 (2003).
38. S. Lagergren, *Sven. Vetenskapsakad. Handingarl.*, **24**, 1 (1898).
39. Y. S. Ho and G. McKay, *Water Res.*, **34**, 735 (2000).
40. W. J. Weber Jr. and J. C. Morris, *J. Sanitary Eng. Division*, **89**, 31 (1963).
41. N. Sarier and Ç. Güler, *J. Am. Oil Chem. Soc.*, **65**, 776 (1988).
42. M. Alkan, Ö. Demirbaş and M. Doğan, *Micropor. Mesopor. Mater.*, **101**, 388 (2007).
43. M. E. Argun, S. Dursun, C. Ozdemir and M. Karatas, *J. Hazard. Mater.*, **141**, 77 (2007).
44. I. A. W. Tan, B. H. Hameed and A. L. Ahmad, *Chem. Eng. J.*, **127**, 111 (2007).
45. F. C. Wu, R. L. Tseng and R. S. Juang, *J. Colloid Interface Sci.*, **283**, 49 (2005).
46. V. C. Srivastava, I. D. Mall and I. M. Mishra, *J. Hazard. Mater.*, **134**, 257 (2006).
47. B. E. Wang, Y. Y. Hu, L. Xie and L. Peng, *Bioresour. Technol.*, **99**, 794 (2008).
48. E. Sabah, M. Çinar and M. S. Çelik, *Food Chem.*, **100**, 1661 (2007).
49. A. K. Biswas, J. Sahoo and M. K. Chatli, *LWT - Food Sci. Technol.*, **44**, 1809 (2011).
50. N. Zhang, H. Qiu, Y. Si, W. Wang and J. Gao, *Carbon*, **49**, 827 (2011).